Advanced Photonics Congress (IPR, Networks, NOMA, PVLED, SPPCom) © OSA 2021

Gallium Arsenide Photonic Integrated Circuit Platform for 1030 nm Applications

Paul Verrinder[1], Lei Wang[1], Joseph Fridlander[1], Fengqiao Sang[1], Victoria Rosborough[1], Michael Nickerson[1], Guangning Yang[2], Mark Stephen[2], Larry Coldren[1], Jonathan Klamkin[1]

Electrical and Computer Engineering Department, University of California, Santa Barbara, CA 93106 USA
NASA Goddard Space Flight Center, Greenbelt, MD 20771 USA
pverrinder@ucsb.edu

Abstract: An active-passive integration platform on GaAs is demonstrated with Fabry Perot lasers exhibiting up to 240 mW total output power, 98.8% injection efficiency, and 3.44 cm^{-1} active loss for operation near 1030 nm.

1. Introduction

Photonic integrated circuits (PICs) allow for the monolithic integration of both active photonic devices such as lasers, modulators, photodetectors, and amplifiers, as well as passive devices. PICs enable a significant reduction in system size, weight and power compared to systems constructed with discrete components. To date, indium phosphide (InP) is the most common PIC platform and is leveraged primarily for telecommunications and data center communications [1]. Recently, InP PICs have begun to impact other areas including free space laser communications, 3D mapping Lidar, and remote gas sensing Lidar [2-5]. Silicon photonics (SiPh) has also matured significantly for communications applications [2]. Outside of the 1310 nm and 1550 nm spectral ranges commonly used for telecommunications, there are other applications that could benefit from the advantages offered by PIC technology. The spectral region near 1000 nm, for example, is heavily utilized. One particular application of interest is airborne topographical Lidar where the form factor of PIC technology would enable deployment on small space platforms [6]. The focus of this work is the development of an active-passive integration platform on gallium arsenide (GaAs) for operation near 1030 nm. GaAs based lasers have been studied for many years, with indium gallium arsenide (InGaAs) quantum wells (QWs) being used for emission wavelengths in the 880-1100 nm range [7]. However, the primary focus in recent years, especially in the longer wavelengths greater than 1000 nm, has been on high power laser diodes or distributed feedback (DFB) and distributed Bragg reflector (DBR) lasers with surface etched gratings [8,9], rather than active-passive integration or widely tunable lasers. The work presented here demonstrates a technique for integrating 1030 nm InGaAs/GaAs QW Fabry Perot (FP) lasers with passive waveguides. This lays a foundation for future development of PIC technology operating near 1000 nm.

2. Material Design and Device Fabrication

The active region consists of three 5 nm $In_xGa_{1-x}As$ (x = 0.271) QWs surrounded by 8 nm $Ga_{1-x}AsP_x$ (x = 0.1) barriers, and GaAs separate confinement heterostructure (SCH) layers. The upper and lower cladding layers are $Al_xGa_{1-x}As$. Active-passive integration is accomplished by growing a partial structure that doesn't include the upper cladding, selectively removing the QW active layers, and then subsequently performing a regrowth of the upper p-cladding and p-contact layer by metalorganic chemical vapor deposition (MOCVD).

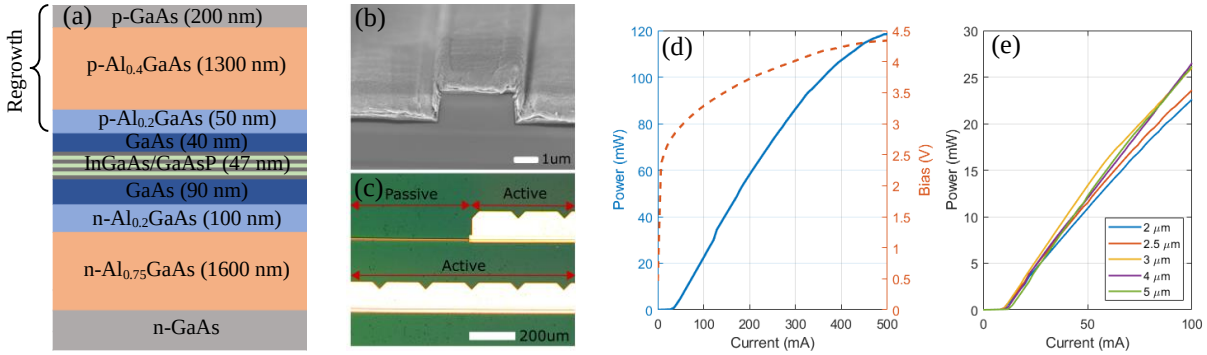

Fig. 1. (a) Layer structure in active section following regrowth. (b) SEM cross section of a cleaved facet 3 µm wide laser and (c) top view optical microscope image of active-passive and all-active FP lasers. (d) Power output from one side of 20x800 μm^2 broad area laser and (e) power from one side of 600 µm long narrow ridge 2-5 µm lasers.

Figure 1(a) reports the layer structure in the active section following regrowth. The QWs are placed closer to the top within the guiding layers, rather than in the middle, to minimize the height of the offset between the active and passive regions. This also allows for efficient optical coupling between the active and passive regions, while still allowing for sufficient overlap between the optical mode and the QWs in the active region. From simulations, the QW confinement factor, Γ_{QW}, is 5.02%, and 96% of the fundamental mode power is coupled from the active region to the passive region. Figures 1(b) and 1(c) show images of fully fabricated devices.

3. Measurement Results

Multiple lasers of varying widths were fabricated, including 20 µm wide broad area lasers, and 2 µm, 2.5 µm, 3 µm, 4 µm, and 5 µm narrow ridge devices with both active and passive sections. These devices were tested under both continuous wave (CW) and pulsed current operation to extract material parameters and device performance characteristics. Figures 1(d) and 1(e) show single sided light-current (LI) characteristics for the 20 µm broad area lasers, and for five different narrow ridge devices, respectively, under CW operation at room temperature. To extract internal loss and quantum efficiency, the broad area devices were tested under pulsed current operation (to mitigate self heating) for various cavity lengths. The inverse of the measured differential efficiency, η_d, is plotted as a function of cavity length with a linear curve fit in Fig. 2(a) to extract internal loss and injection efficiency values of 3.44 cm^{-1} and 98.8%, respectively. Similar measurements were obtained for active-passive FP lasers to extract a passive waveguide loss of 4.05 cm^{-1}. Figure 2(b) shows the spectral output of a 3 µm wide laser at several different CW current injection levels.

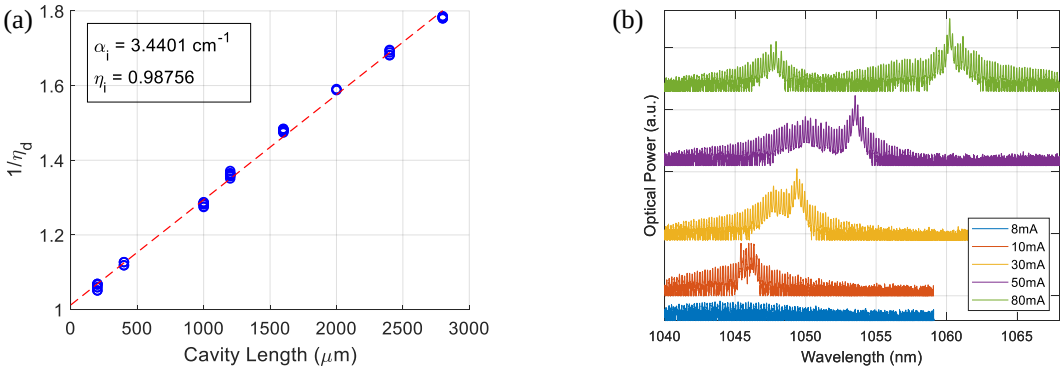

Fig. 2. (a) Inverse of measured differential efficiency as a function of cavity length for 20 µm broad area lasers. (b) Optical spectra under CW current injection for 3 µm wide lasers.

4. Conclusions

An active-passive GaAs PIC platform for 1030 nm operation has been demonstrated. FP lasers were integrated with passive waveguides, demonstrating up to 240 mW total power output from broad area devices, and greater than 50 mW out of narrow ridge devices at 100 mA CW current injection. These devices exhibit state-of-the-art laser performance characteristics with 3.44 cm^{-1} internal loss, 98.8% injection efficiency, 85.5 A/cm^2 transparency current density, and threshold current as low as 9 mA.

5. Acknowledgements

The authors acknowledge funding support from the NASA ESTO Advance Component Technology program.

6. References

[1] F. Kish, *et al.*, *Proc. IEEE*, vol. 101, no. 10, pp. 2255–2270, 2013
[2] J. Klamkin, *et al.*, *Opt. Express*, vol. 22, no. 2, p. 2150, 2014
[3] J. Fridlander, *et al*, Conference on Lasers and Electro-Optics (CLEO) 2020.
[4] H. Zhao *et al.*, *IEEE J. Sel. Top. Quantum Electron.*, vol. 24, no. 6, pp. 1–6, 2018
[5] B. J. Isaac, *et al*, *IEEE J. Sel. Top. Quantum Electron.*, vol. 25, no. 6, pp. 1–7, 2019
[6] A. W. Yu, *et al*, Proc. SPIE 8599, 85990P (2013)
[7] J. J. Coleman, *Journal on Selected Topics in Quantum Electronics*, vol. 6, no. 6, pp. 1008–1013, 2000
[8] A. Pietrzak, *et al*, Proc. SPIE 10900, 109000K (2019)
[9] S. Spieberger, *et al*, *Appl. Phys. B Lasers Opt.*, vol. 104, no. 4, pp. 813–818, 2011